HHS Public Access

Author manuscript

J Immunol. Author manuscript; available in PMC 2019 May 01.

Published in final edited form as:

J Immunol. 2018 May 01; 200(9): 3231–3243. doi:10.4049/jimmunol.1701500.

Single degranulations in Natural Killer cells can mediate target cell killing

Lavesh A. Gwalani and **Jordan S. Orange**

Department of Pathology and Immunology, Baylor College of Medicine and The Center for Human Immunobiology, Texas Children's Hospital, Houston, TX 77030, USA

Abstract

Natural killer (NK) cells are cytotoxic lymphocytes important in defense against viral infection and cancer. NK cells mediate cytotoxicity predominantly through directed secretion of lytic granules which are specialized lysosome-related organelles, containing effector molecules such as perforin and granzymes. Although many requirements for lytic granule transport to and secretion at the NK cell lytic synapse are known, the minimum number of degranulation events required by an NK cell to kill its target is unknown. We performed high-resolution four-dimensional confocal microscopy of human NK-target cell conjugates to quantify NK cell degranulation (using a degranulation indicator, LAMP1-pHluorin) as well as target cell death. Despite containing over 200 granules, we found that an individual NK cell needed only 2 to 4 degranulation events, on average, to mediate target cell death. Although NK cells released approximately one-tenth of their total lytic granule reserve upon a single target they required just over one-hundredth of their total lytic granules to kill a target cell. Importantly, the kinetics of NK cell killing correlated to the size of and the amount of effector molecules contained within lytic granules, as well as the temporal, but not spatial organization of degranulation events. Thus our study answers a fundamental question as to how many degranulation events it takes for a human NK cell to kill its target.

Keywords

Lytic granules; Cytotoxicity; LAMP1; Live cell imaging; Immunological synapse

INTRODUCTION

NK cells mediate cytotoxicity against virally infected and cancerous cells while also producing a variety of chemokines and cytokines that influence other immune cells (1, 2). Given that NK cells are a formidable defense against malignancy, their therapeutic use in anti-tumor immunotherapy is being advanced in clinical trials (3). Promising approaches to use NK-cell based immunotherapy include autologous NK cells, allogeneic NK cells, NK cell lines and chimeric antigen receptor (CAR)-transduced NK cells (3). All of these approaches are believed to take advantage of and rely upon the cytotoxic capacity of NK cells and their ability to kill tumor cells. The most successful use of NK cells, as adoptive immunotherapy, will require a deeper understanding of the complex biology that comprises

Corresponding author: Jordan S. Orange (orange@bcm.edu).

killing activity of NK cells. With regards to the mechanics and cell biological mechanisms of NK cell cytotoxicity, there are many unanswered questions including the minimum cellular requirements for an NK cell to kill a susceptible target cell.

NK cells kill their targets predominantly by releasing the contents of preformed lysosomal-related organelles known as lytic granules (4). The exocytosis of lytic granules is a tightly regulated process beginning with conjugation of an NK cell with its target cell to form an immunological synapse (IS) at the contact site (5, 6). The lytic granules undergo transport on microtubules converging towards the microtubule-organizing center (MTOC), which serves to prevent them from being released outside of the IS (7, 8). Temporal and spatial integration of signals at the lytic IS between the NK cell and its target cell lead to rearrangement of the actin cytoskeleton followed by polarization of the MTOC and the lytic granules towards the IS to allow for focused release onto the target cell (7–10). The lytic granules dock at the plasma membrane before finally fusing with the plasma membrane and releasing their cytotoxic contents at the IS (11–13); a process termed degranulation. This is followed by the released lytic granule contents acting upon the target cell resulting in its death. Thereafter, the NK cell disengages from the killed target, at which point the NK cell may mediate serial kills eradicating additional target cells (14) .

A focus of research has been to unravel the molecular mechanisms governing key regulatory steps in the lytic granule exocytosis pathway. Many critical checkpoints have been identified as well as the signals leading up to and allowing passage through them (6). While these culminate in degranulation as is frequently measured as a hallmark of NK cell activity, the quantitative requirements for this function are unclear. More specifically, the number of degranulation events in individual NK cells needed for target cell death is a fundamental question that remains unanswered. Furthermore, the functional relevance of any specific number of degranulation events in determining the outcome of interactions between NK cells and their targets at a single cell level is unknown.

The standard measure of NK cell killing activity is the “gold standard” ^{51}Cr-release cytotoxicity assay (15) which is augmented by a variety of flow cytometry based assays (16). These assays measure NK cell killing but do not measure the killing ability of a single NK cell or the dynamics of the cytotoxic process. We used high resolution confocal microscopy to measure degranulation events during a single NK cell’s interaction with its target to better understand the quantitative relationship between degranulation and the dynamics of NK cell killing.

The lysosomal-associated membrane protein-1 (LAMP1/CD107a) is widely used as an indicator of NK-cell degranulation as it appears on the cell surface due to fusion of lysosomes with the plasma membrane (17–19). We used a previously designed LAMP1 fusion protein with pHluorin, the pH sensitive variant of the GFP (20, 21), to obtain stable expression of an indicator of degranulation in NK cell lines. The typical acidic conditions in the lytic granules contained within NK cells keep the pHluorin fluorescence masked, but as the lytic granules fuse with the NK cell synaptic membrane, the acidity of lytic granules is lost and pHluorin encounters a neutral pH environment and can fluoresce under green light. This system has allowed for the sensitive detection of single degranulation events (20, 21)

In this present study, we utilized high resolution confocal microscopy in live NK cells to quantify degranulation events throughout 3-dimensions between the NK cells expressing LAMP1-pHluorin in conjugation with susceptible target cells. We found that, at a single cell level, an NK cell kills its target using a surprisingly low number of degranulations, representing a small fraction of the total NK cell lytic granule content. Characterization of the lytic granules contained within the NK cells and the degranulation events that lead to target cell death further demonstrated that the efficiency and kinetics of target cell killing by NK cells related not only to the number of degranulations but also to the size of the lytic granules, their effector molecule density and the speed with which the lytic granules were released at the NK cell IS.

MATERIALS and METHODS

Cell lines and Primary human NK cells

LAMP-1-pHluorin transduced human NK cell lines NK92 and YTS were generated as described (20). The NK cell lines NK92 and YTS, and the target cell line 721.221 cells were maintained in culture as described (20, 22). Ex vivo NK cells (eNK) were isolated from concentrated human blood using RosetteSep™ Human NK Cell Enrichment Cocktail (Stemcell Technologies) and were used in live cell cytotoxicity assays. RosetteSep™ enriched or $CD56^{+}$ $CD3^{-}$ flow sorted primary human NK cells were expanded in-vitro as described previously (22). LAMP-1-pHluorin transduction of in-vitro expanded primary human NK cells was performed using a protocol similar to the one used for transduction of human NK cell lines (20). LAMP-1-pHluorin positive primary human NK cells were flow sorted, further expanded in-vitro and were subsequently used in live cell cytotoxicity assays.

Live cell cytotoxicity assay

For live cell imaging, the LAMP-1-pHluorin transduced human NK cell lines NK92 and YTS (effectors) were prepared by staining with 1μM of LysoTracker Deep Red (ThermoFischer Scientific) for 30 minutes at 37°C and washed twice with warm phenol red free RPMI medium supplemented with 10%FBS (imaging medium). The target cell line 721.221 was prepared by staining with1μM of Calcein Red-Orange, AM (ThermoFischer Scientific) in serum free imaging medium for 10 minutes at 37°C and washed. ΔT dishes (Bioptechs) were prepared by coating with 5ug/ml of mouse anti-human CD48 antibody (Clone TU145 BD Biosciences) for 60 minutes at 37°C and washed with imaging medium to remove unbound antibody. The effector and target cells were mixed in imaging medium at a 2:1 ratio in the ΔT dish and immediately placed on the stage top 37°C incubator (Pathology Devices Inc.) of a Zeiss Axioplan Observer Z1 microscope with a Yokogawa CSU10 spinning disk and a Hamamatsu Orca-R2 C10600 CCD camera. After 5 minutes of incubation, a single cell conjugate between the NK and its target cell was selected and time lapse images acquired. The NK cell was identified by LysoTracker stained granules and the target cells were identified by their calcein staining. Even though target cells were not stained with LysoTracker, some the excess dye from the NK cells that leaked back in to the medium was taken up by the target cells and most of the target cells were positive for both calcein and LysoTracker dyes. This phenomenon was confirmed through specific control experiments using both lysotracker labeled and unlabeled YTS cells.

Image acquisition began within 10 minutes of effector –target cell incubation and was considered as time zero for image analysis. Imaging was performed using the plan apochromatic 63× 1.4NA oil immersion objective. Laser lines used included 488, 561, and 637 nm Coherent OBIS LX (Santa Clara, CA), housed and powered using a MultiLine LaserBank and controller (Cairn Research, Faversham, UK). Motorized stage (LEP 96S107-Z3-RE) and filter wheel (LEP 99A351) were controlled by an LEP MAC6000 unit (all from Ludl Electronic Products Ltd., Hawthorne, NY). Imaging for live cell cytotoxicity assays was optimized at a frame rate of one image every 2.4 minutes for 90 to 120 minutes until target cell death was observed as evidenced by complete loss of calcein fluorescence and appearance of morphological changes in the target cell. Images were captured at 5 *z*-axis planes focused on the NK cell and a single reference *z*-axis plane focused on the target cell. Images were acquired using the Volocity3D (PerkinElmer) or Metamorph 3D (Molecular Devices) image acquisition software.

For photo-ablation of effector cells during live cell imaging, the YTS cells (effectors) and 721.221(targets) were prepared for live cell imaging as above. Chamber slides (Lab-Tek) were prepared by coating with 5ug/ml of mouse anti-human CD48. The effector and target cells were mixed in imaging medium at a 2:1 ratio in the chamber slides and immediately placed in the incubation chamber (maintained to 37°C) of a Leica SP8 laser scanning confocal fluorescence microscope. After 5 minutes of incubation, a single cell conjugate between the NK and its target cell was selected and time lapse images acquired. Imaging was performed with 100X 1.45 NA objective with excitation by a white light laser at 496, 568 and 647nm. To affect photo-ablation of the effector YTS cell, Argon laser pulses at 405nm with 80% intensity were applied to the region of the YTS cell either before or after the lytic granules had polarized to the target cell. 20 pulses were applied over duration of 5 minutes. Live cell imaging was resumed after application of photo-ablation laser pulses for a duration of 60 to 90 minutes. Images were acquired using *z*-axis planes at every 500nm from the top to the bottom of the cell using the Leica LAX application suite.

Fixed cell imaging

For fixed cell imaging, LAMP-1-pHluorin transduced human NK cell lines (NK92 and YTS) were plated on warmed Silane coated slides (Electron Microscopy Sciences) and fixed/permeabilized using the Cytofix/Cytoperm kit (BD Biosciences). Cells were then stained with Alexa Fluor 647 anti-human perforin antibody (Clone δG9 Biolegend) for 60 minutes at 37°C, washed with perm/wash buffer and mounted overnight in ProLong Gold antifade mounting medium (ThermoFischer). Imaging was performed on the Leica SP8 laser scanning confocal microscope with a 100X 1.45 NA objective with excitation by a white light laser at 496 nm and 647nm and emission detected by HyD detectors. Images were acquired with *z*-axis planes every 120nm from top to the bottom of the cell.

Image analysis

Image analysis was performed using Volocity3D image analysis software (PerkinElmer). Live cell time-lapse images were cropped to the selected single cell conjugate and thresholded using fluorescence intensity in the respective channels to remove background and nonspecific fluorescence. Degranulation events were measured in the synaptic region of

interest (ROI) drawn on the region of the overlap between NK and its target cell observed in bright field illumination. Due to the dynamism of the degranulation signal, degranulation events were measured at each time point. Every additional degranulation event measured was cumulatively added to an already measured event from a previous time point and a cumulative frequency of degranulation events were plotted. Total calcein fluorescence was measured in the target cell as a sum of all the volumes multiplied by the mean fluorescence intensity at each time point and plotted as a percentage of maximum total fluorescence intensity observed during the imaging period.

For fixed cell images, deconvolution was performed using the Huygens Professional software suite (Scientific Volume imaging). Images were then converted to a format compatible with Volocity3D and image analysis for measurements of lytic granule number was performed using Volocity3D image analysis software.

Isolation of NK lytic granules

Lytic granules were isolated from the NK cell lines using the Thermo Scientific™ lysosome enrichment kit as previously described previously (22).

Western Blots

For Western blot analysis, the isolated lytic granules were pelleted and solubilized in 30 to 100μl of 1X CHAPS cell extract buffer (Cell Signaling Technologies) supplemented with 1X Halt™ protease inhibitor cocktail (ThermoFischer Scientific), incubated at room temperature for 10 mins, vortexed and directly used. Lytic granule lysates from approximately 10×10^6 cell equivalents were first boiled with NuPAGE LDS sample buffer (Novex-ThermoFischer Scientific) and NuPAGE sample reducing agent (ThermoFischer Scientific) before applying to a column of NuPAGE 4-12% Bis-Tris density gradient gel (ThermoFischer Scientific). The separated proteins on the gels were transferred in an XCell II™ Blot Module onto nitrocellulose membranes (Novex-ThermoFischer Scientific) which were then blocked with 5% non-fat milk in PBS/0.05% Tween20 (PBST) for 60 minutes at room temperature. The membranes were then incubated with the following primary antibodies in 5% bovine serum albumin in PBST: anti-perforin 1: 500 (mouse monoclonal BD48 – Abcam), anti- granzymeB 1:1000 (rabbit polyclonal – Abcam), anti-LAMP1 1:500 (mouse anti-human antibody; clone 25 BD Biosciences). Myosin IIA 1:1000 (rabbit anti-myosin IIA Sigma-Aldrich) was blotted as loading control. The bound primary antibodies were then probed with anti-mouse or anti-rabbit IRDye secondary antibodies (Li-COR) and the membranes were imaged using the Odyssey® CLx imaging system (LI-COR Biosciences). Analysis of western blot images and densitometry was performed using the Image Studio Lite software.

Flow cytometry

Flow cytometry was performed on isolated lytic granules from LAMP-1-pHluorin transduced NK cell lines. The lytic granules were fixed and permeabilized using the Cytofix/Cytoperm kit (BD Biosciences) and then stained with PE-Cy5 labeled mouse anti-human CD107a antibody (Clone H4A3 eBiosciences) antibody. Subsequently the stained granule

were washed in PBS/1%FBS twice at 18000×g and acquired on a BD LSR-II Fortessa flow cytometer.

^{51}Cr release cytotoxicity assay

Cytotoxicity assays using the NK cell lines as effector cells and 721.221 cells as target cells and measurement of specific lysis were performed as described previously(22).

Statistics

Statistical analyses were performed using Graphpad Prism6. Unless otherwise noted, all analyzes utilized either Student's *t*-Test or one way Anova with correction for multiple comparisons. Differences in measurements were considered statistically significant when the *p*-value was less than 0.05.

RESULTS

Calcein as an indicator of cell death in live cell imaging assays

The number of degranulation events in an NK cell required to mediate killing of a single target cell is unknown. Using high-resolution live-cell imaging we wanted to define the minimum number of NK cell degranulations needed for target cell death. A number of different approaches have been used to visualize target cell death at a single cell level in live cell imaging experiments (23). These can be specific for: 1) activation of cell death pathways; 2) rupture of cell membranes or 3) loss of nuclear integrity. Since we wanted to determine the minimum number of degranulation events used by an NK cell to kill its target, we sought a cell death indicator that would enable us to determine an early point in the initiation of cell death. We selected the vital dye Calcein-AM as its extinction from target cells in cytotoxicity assays has been shown to be comparable to the "gold standard" of ^{51}Cr-release (24–27). Calcein-AM is a highly cell permeable acetoxymethyl ester of calcein which is cleaved by cellular esterases to remove the AM group to gain fluorescence properties and become impermeant to the cell membrane. As such, the loss of calcein fluorescence is an indicator of cell death.

In order to evaluate the kinetics of calcein loss as compared to nuclear permeabilization as measures of cell death we imaged target cells loaded with Calcein-AM in media that contained SYTOX Green nucleic acid dye in the presence of NK cells. YTS NK cells (28) that contained a LAMP1-pHluorin degranulation indicator (hereafter referred to as "YTS" cells) were incubated with calcein orange-red labeled 721.221 target cells at a 2:1 effector: target ratio in a 37°C temperature controlled stage-top incubator of a spinning disc confocal microscope capable of resolution approaching 200nm. NK-target cell conjugates were imaged for 120 to 180 minutes until target cell death was observed. Loss of calcein fluorescence by a representative target cell was identified as an early event after conjugate formation and was almost always accompanied by morphological changes in the membranes of the target cell. These changes were characterized by membrane blebbing, contraction, and subsequent swelling of the target cell and only thereafter was SYTOX entry visualized (Figure 1A and Suppl. Video1). Quantitative analysis of time-lapse images of this particular representative conjugate demonstrated that loss of calcein fluorescence from the target cell

preceded the gain of SYTOX fluorescence (Figure 1B). Thus we pursued the loss of calcein fluorescence as a cell death indicator in our live cell cytotoxicity assays to determine the earliest degranulation events that could lead to target cell death.

Calcein fluorescence as an indicator of cell death, however, is known to be complicated by spontaneous loss of calcein from target cell lines resulting in a limited dynamic range of specific release for the assay (29). In order to define this in our system, we determined the spontaneous loss of calcein fluorescence by the 721.221 target cell line by imaging these cells after calcein labeling in the absence of effector NK cells. Over the 90 min duration of time-lapse imaging, 721.221 cells gradually lost 60% of calcein fluorescence intensity (Figure 1C). The loss of calcein fluorescence in the 721.221 cells in these assays, however, was never accompanied by morphological changes indicative of cell death (Suppl. Video 2). Thus accelerated loss of calcein fluorescence in the target cell, when in concert with morphological changes, was considered as a reliable indicator of target cell killing by NK cells in our live cell imaging experiments.

Minimal degranulation in an NK cell initiates killing of single target cells

In order to determine the number, kinetics and orientation of NK cell degranulations that lead to the killing of a target cell, we imaged YTS cells in conjugation with 721.221 target cells over 90 min using maximal image capture rates through 3-dimensions that specifically minimize photo-toxicity and photo-bleaching. YTS cells were labeled with LysoTracker™ Deep Red and mixed with calcein orange-red labeled 721.221 target cells at a 2:1 ratio. While lytic granules could be identified throughout imaging as red fluorescent organelles in the NK cells, as the imaging progressed green fluorescent events appeared in the synaptic region and were identified as degranulation events. The appearance of degranulation was followed by loss of calcein fluorescence from and subsequently morphologic change in the 721.221 target cell (Figure 2A and Suppl. Video 3). Quantitation of the cumulative frequency of degranulation events in the YTS cell and comparison to the sum total intensity of calcein fluorescence (as a percent of maximal fluorescence in the 721.221 target cell) demonstrated that the initial degranulation event was associated with the majority loss of calcein fluorescence (Figure 2C). This suggested that minimal NK cell degranulation could be promoting target cell destruction.

To confirm that limited NK cell degranulation promotes target cell death and to ensure that this was generalizable beyond the YTS cell line, we used a different human NK cell line, NK92 (30) expressing the LAMP1-pHluorin degranulation indicator (hereafter referred to as “NK92” cells). In similarly designed time-lapse experiments the ability of NK92- cells to kill 721.221 was evaluated. Akin to that observed in YTS -721.221 conjugates, degranulation events in the NK92 cell were followed by loss of calcein fluorescence in the 721.221 target cell along with appearance of the target cell membrane blebbing (Figure 2B and Suppl. Video 4). Quantitative analysis of the cumulative degranulation frequency and calcein fluorescence extinction kinetics in this representative conjugate demonstrated that a single degranulation event in the NK92 cell was associated with a major loss of target cell calcein fluorescence and a few additional degranulation events were observed before complete extinction (Figure 2D). Similar to our observation with NK cell lines, calcein

fluorescence extinction in target cells and the associated kinetics of degranulation were also identified when primary human NK cells were used as effector cells. LAMP-1-pHluorin was transduced into primary human NK cells, which were conjugated with 721.221 target cells and observed in time-lapse experiments. A little as a single degranulation event initiated the loss of calcein fluorescence and only a few additional degranulation events were observed before major calcein fluorescence loss and target cell blebbing (Supplemental Figure 1). Thus, at a single cell level, NK cells can kill their target cells via minimal degranulation events.

NK cells use only a fraction of their lytic granules to kill a target cell

In light of the single cell observations of degranulation and death we next wanted to quantitatively determine the number of degranulation events utilized by an NK cell to kill its target cell. Thus, we performed time-lapse 3-dimensional imaging using multiple single-cell conjugates between NK and target cells. Death of 721.221 target cells mediated by YTS cells demonstrated two distinct patterns of calcein fluorescence loss following the first observed degranulation event: abrupt and gradual (Figure 3A). Similar to that identified in previous studies of NK cell cytotoxicity (31) we termed these distinct patterns mediated by YTS cells as either “fast killing” or “slow killing” (Figure 3A). Interestingly, NK92 cells did not demonstrate bimodal killing kinetics and instead were in between the “fast” and “slow” killing mediated by the YTS cells (Figure 3B). Similar calcein fluorescence extinction kinetics and the fast and slow killing patterns of target cell killing were also observed when primary human NK cells were used as effector cells against the 721.221 target cells in live cell time-lapse experiments (Supplemental Figure 2).

In order to generate a single quantitative measure of killing we considered the spontaneous loss of calcein (likely photobleaching, which did not exceed 60%) of total to define the loss of >60% as a threshold for commitment to cell death, when also accompanied by or followed by morphological changes in the target cell. Using this measurement, the minimal number of NK cell degranulations that effectively killed a 721.221 target cell were 2±1.4 for fast and 4±3.4 for slow killing by YTS cells and 3±2.8 for killing by NK92 cells (Figure 3C). Thus, in two different human NK cell lines the average minimum number of degranulation events required to kill a single target cell was in the range of 2 to 4.

Even though nearly all of an NK cell’s lytic granules were polarized towards the lytic synapse formed with the target cell, we observed that only a few degranulate. This suggests that only a fraction of an NK cell’s granules are released onto a target cell in any individual killing interaction. To understand the relation between total number of lytic granules contained in an NK cell, those that degranulate and the minimal number required to kill a target cell we quantified the lytic granule content of both YTS and NK92 cells. We performed three-dimensional high resolution laser scanning confocal fluorescence microscopy on fixed NK cells to enumerate lytic granules using either the LAMP-1-pHluorin signal or perforin staining. The number of lytic granules based on perforin staining was similar to the number obtained using the LAMP-1-pHluorin signal (Figure 3D). A slightly higher number of lytic granules were measured using the LAMP-1-pHluorin signal. This is most likely due to the LAMP-1-pHluorin signal being detected in predecessors to

lytic granules, which lack the mature form of perforin. YTS and NK92 cells contained an average of 194±51and 206±57 perforin positive lytic granules, respectively. Primary human NK cells contained an average of 63±23 lytic granules (Supplemental Figure 2), which although different form the NK cell lines, was not surprising given the smaller size of primary cells. The maximal number of lytic granules released in a single conjugation event as determined by the degranulations in the synaptic region of the NK-target cell conjugate in live cell imaging assays was 16±8 and 12±7 for YTS and NK92 cells, respectively. Thus upon forming a lytic immunological synapse NK cells release approximately one-tenth of their total lytic granule content onto the target cell, but may require as low as one-hundredth of their total lytic granules to kill their target cell (Figure 3E).

Even though 2 to 4 NK degranulations were effective in causing over 60% calcein loss in target cells, we observed additional degranulation events in the synaptic region, even after appearance of morphologic changes in the target cell. To ensure that the initial 2 to 4 degranulation events in the NK cells were sufficient to kill the target cell and that the target cell endured irreversible damage during this initial time interval, we disrupted the YTS-721.221 cell conjugate by photo-ablating the YTS NK cell right after lytic granules polarized towards the IS and calcein had begun to leak from the target. Specifically, we destroyed the YTS cell using focused high intensity UV pulses directed at only the NK cell after granule polarization occurred and calcein loss began. This photo-ablation procedure led to immediate deformation of the YTS cell and its eventual blebbing. Despite the destruction of the YTS cell via photo-ablation, however, the target cell continued to lose its calcein and underwent morphological changes indicative of cell death (Figure 4A, B and Suppl. Video 5). As a control, the YTS cell was photo-ablated earlier in the conjugate formation process before the lytic granules polarized towards the IS and before calcein extinction had begun. Such disruption prevented the accelerated loss of calcein fluorescence (Figure 4B) as well as any morphological changes in the target cell. Thus membrane integrity loss in the target cell due to initial NK degranulations was irreparable and sufficient to allow for target cell death.

Relative differences in lytic granule size and content relate to killing efficiency

Since at a single cell level we observed kinetic and efficiency differences in target cell killing between the YTS and NK92 cells, we wanted to determine if this might be due to an inherent characteristic of the different NK cells themselves. The disparity in killing effectiveness between YTS and NK92 cells was also identified at a population level in standard ^{51}Cr release cytotoxicity assays, with the former having significantly higher killing of 721.221 target cells compared to the latter (Figure 5A). One explanation for potency differences between YTS and NK92 cells could be because of specific properties of the lytic granules themselves. To evaluate this possibility we isolated lytic granules from each of the NK cell lines using density gradient ultracentrifugation (22) and compared their characteristics. We first stained isolated lytic granules using anti-LAMP-1 antibody and performed flow cytometric analyses. Forward scatter comparison of the LAMP-1 positive lytic granules indicated that those from YTS were larger than those from NK92 cells (Figure 5B). To determine if this size disparity correlated with a difference in cytolytic effector content, lytic granules from a fixed number of YTS and NK92 cells were lysed and contents separated via electrophoresis under denaturing conditions and then evaluated via Western

blot analysis using antibodies specific for perforin and granzymeB. Both perforin and granzymeB were identified at higher levels in the YTS cell lytic granules (Figure 5C). Since the lytic granules were prepared from the same number of cells and there are essentially the same numbers of lytic granules per cell (Figure 3D) the YTS granules can be considered to have greater cytolytic molecule content per granule. Thus, differences in the overall cytotoxic efficiency between the YTS and the NK92 were likely a feature of lytic granule size and the quantity of cytolytic effector molecules contained in the lytic granules themselves.

Spatiotemporal organization of NK cell degranulation and efficiency of individual target cell killing

While differences in the lytic granules between YTS and NK92 cells may explain the difference in the number of degranulations needed to kill a target cell between the two cell lines, they do not explain the observed fast and slow killing mediated by the YTS cells. Our initial hypothesis for the kinetic difference was that the spatial relation of degranulation relative to the lytic synapse was going to be a determining factor. Prior studies have identified a “lytic cleft” as a potentially protected zone of the lytic synapse specialized for promoting target cell death (32) and thus we speculated that degranulation closer to the center of the synapse within the presumed lytic cleft would translate to greater lytic effectiveness. To evaluate this possibility we performed three-dimensional time-lapse imaging of the interaction between NK cells and their targets and measured the distance of individual degranulation events from the centroid of the lytic synapse, which we then related to target cell calcein extinction. The three-dimensional distances between the degranulation events and the centroid of the synaptic region in conjugates between YTS, or NK92 and 721.221 target cells demonstrated a range of distances throughout the synapse. When each distance was normalized to the size of the synapse in which that degranulation was measured, there were no significant differences of the mean of each of the two cell lines (Figure 6A). The overall mean synapse sizes were also not different (Figure 6B). More importantly, however, the distance of the degranulations from the centroid of the synapse when normalized to the size of the synapse did not distinguish the fast from the slow killing subsets of the YTS cells (Figure 6A). Thus, it seemed unlikely that the spatial characteristics of degranulation within the synapse were relevant to killing efficiency.

A second hypothesis for the dichotomy in NK cell killing kinetics and efficiency on a single cell level is more simply that it relates to the temporal organization of degranulation. To evaluate this we measured the time needed to reach the minimal degranulation events required for commitment to target cell death (from Figure 3C) and compared that to the actual time of commitment to death (>60% loss of calcein). For both the YTS and NK92 cells conjugated to 721.221 target cells there was a positive correlation between the time of commitment to target cell death and that to achieve minimal effective degranulation (Figure 6C and D). Importantly in YTS cells, the appearance of rapid degranulation events after conjugate formation resulted in fast killing and a more gradual appearance of degranulations resulted in slow killing of target cells. For the NK92 cells, there was still an association between appearance of degranulation events and target cell death even though there was no overall dichotomy of cell death that allowed for fast and slow killing categories. We also

performed these correlation analyses by evaluating the membrane changes in the target cell as a measure of commitment to death (Figure 6E and F) and verified the positive correlation between degranulation and death similar to using calcein loss as a measure of commitment to death (Figure 6C and D). However, for both the YTS and NK92 cells conjugated to 721.221 target cells the exact location of degranulation within the synaptic cleft did not correlate to the time of commitment to target cell death (>60% loss of calcein) (Figure 6G and H). Thus the number of degranulations, the size and contents of lytic granules and the speed with which the lytic granules are released at the lytic synapse direct the efficiency of target cell killing by NK cells.

DISCUSSION

Live cell imaging assays of single NK-target cell interactions have provided insight in to understanding how NK cells kill (33, 34). NK cells are heterogeneous in their killing ability with some cells being more cytotoxic than others at any given time (33). The process of how an NK cell organizes its lytic machinery is well established, but the number of lytic granules required for the cytotoxic activity has been unknown. Using high-resolution four-dimensional confocal microscopy we determined the minimum number of degranulations required by NK cells to kill single target cells. This also allowed us to correlate the characteristics of lytic granules themselves, the kinetics of degranulation, and the three dimensional orientation of the degranulations to the cytotoxic efficiency of NK cells at a single cell level. We found that a small fraction of NK cell lytic granules were needed to mediate a target cell kill and that the kinetics of degranulation and size of granules was relevant but the positioning of degranulation was not.

We quantified degranulation in NK cells using a pH sensitive degranulation indicator LAMP1-pHluorin (20) in two distinct human NK cell lines (YTS and NK92) and in primary NK cells in concert with using calcein for sensitive detection of target cell death. The MHC-class I negative 721.221 B lymphoblastoid cells were used as a single common target as they are more uniformly susceptible to NK cell killing than K562 target cells (14), and the use of a common target cell allowed us to minimize the influence of target cell characteristics on the cytotoxicity from the two different NK cell lines. When evaluated using time-lapse confocal microscopy visualization and measurement of the entire NK cell kill was possible.

On average, 2 to 4 degranulation events were sufficient for an NK cell to kill its target cell. Interestingly, in some experiments target cells lost most of their calcein and ultimately died from a single degranulation event. Even though target cells lost most of their calcein and demonstrated membrane changes indicative of cell death after these initial fatal degranulations, the NK cells continued to degranulate at the immune synapse and released an average of 12 to 16 lytic granules on to the dying target cell. This difference in the minimal number of degranulation events required for a single target cell kill and the total number of lytic granules exocytosed on to the target cell could be a mechanism in NK cells whereby NK cells release more lytic granules on to the target cell than the minimum required to ensure target cell killing. A simple explanation for this could be that the continued presence of the target cell allows for continued activation signaling for degranulation and that these events continue until the NK cell detaches from the target cell.

The absence of active detachment in our imaging experiments, to be induced either by the complete disintegration of the target cell or by a neighboring target cell, might lead to continued attachment and degranulation observed even after death of the target cell. This would be consistent with recent work demonstrating the active detachment process utilized by NK cells during cytotoxicity and that NK cells maintain their activation status and continue to express markers for degranulation immediately after detachment from the dead target (35).

Following exocytosis, the lytic granules are endocytosed for recycling of its membrane proteins as one of the mechanisms to promote serial killing of target cells (36, 37). Persistence of the degranulation signal after target cell death observed in our experiments, and in some cases, even after detachment of the NK cell from the target cell, however, might be in part due to the inability the lytic granules to acidify after endocytosis as a result of the stress endured by the NK cells in our experimental imaging system. While this might lead to more apparent accumulated degranulations it would not interfere with our observed minimal number of degranulations needed for killing.

Using high resolution fixed cell imaging we further demonstrated that YTS and NK92 cells contained an average of 194 and 206 lytic granules, respectively. In accordance with previous findings (20, 21), we observed that even though NK cells polarize nearly all of their lytic granules towards the lytic immune synapse, the entire lytic granule load does not get exocytosed on to a single target cell. Even in the case of CTLs, it is implied that a small number of their total lytic granules are needed to kill a single target cell (38–40). Quantitative analysis of live single cell interactions between NK cells and their targets in our study demonstrates that while NK cells release approximately 10% of their total lytic granules on to the target they require approximately 1% to kill. This suggests that NK cell lytic granules are extremely efficient and that by not releasing its entire lytic granule reserve on to a single target, an NK cell is able to preserve its capacity for serial killing of multiple targets.

At a single cell level, the kinetics of target cell killing between the YTS and NK92 was different, with the former having a bias towards faster kills. This was largely explicable by two features of the NK cells themselves. The first is that lytic granules from YTS cells were larger and contained higher amounts of effector molecules perforin and granzymeB compared to the lytic granules from NK92 cells, thus likely leading to faster kills for every given degranulation. The second was simply a feature of the kinetics of the degranulation events themselves. Interestingly, YTS induced killing of 721.221 target cells was bimodal. As observed previously (31, 33) majority of the target cells demonstrated slow killing however a minor proportion of target cells were killed quickly. While again, this related to the kinetics of the degranulations it is important to consider that NK cells induce two cytotoxic pathways in their target cells (41, 42). Apoptosis is the primary mechanism of target cell death initiated by granzymes and mediated by the caspase pathway of apoptosis. However a small proportion of NK cells kill their target cells by inducing necrosis in their targets mediated by perforin induced osmotic lysis. Also when apoptosis is inhibited, the proportion of targets that undergo necrosis increases (41, 42). The patterns of loss of viability in the 721.221 target cells when conjugated to the YTS cells are most likely a

reflection of the two mechanisms of killing by NK cells. Even though majority of the YTS cells induced the apoptotic or slow mode of killing, the higher amounts of perforin released on to target cells via the larger granules in the YTS cells may be high enough in a small proportion of target cells to bias towards necrotic or fast mode of killing. In NK92 cells, the release of relatively lower quantities of lytic granule effector molecules initiated only apoptosis of target cells and could explain the lack of fast mode of killing.

We had initially hypothesized that the spatial relationship of the degranulation to the lytic synapse and target cells would also be a relevant factor. Canonically, lytic granules in CTL are thought to be secreted in a central secretory domain of the immune synapse and the spatial organization of lytic granules within the secretory domain (as well as the kinetics of their delivery to the synapse) have been related to the CTL's killing efficiency (9, 43, 44). Our measurements of distances between individual degranulation events and the centroid of the respective immune synapses did not define differences between the YTS and NK92 cells and did not correlate to the rate of calcein extinction from target cells. Thus, the exact point of lytic granule exocytosis and its three-dimensional orientation in relation to the immune synapse is not a determining factor in the kinetics and efficiency of NK cell killing. This may be a feature of the observed diffuse actin meshwork at the NK cell lytic synapse and the lack of degranulation in any definable isolated secretory domain (20, 43). It is unclear at present whether this represents a defined distinction between NK cells and CTLs, but it is possible that T cell signaling more specifically promotes use and definition of a secretory domain at the synapse. It is increasingly clear, however, that a diffuse actin mesh exists at both the NK cell and T cell synapse (20, 45, 46).

All measures of degranulation in this study were defined from human NK cell lines YTS and NK92, which even though are established models to study NK cell biology (47), the question remains if these measures can be directly applied to primary human NK cells. In addition to the limitation of maintaining primary cells in culture, a major challenge of using primary NK cells was the difficulty of introducing the LAMP1-pHluorin vector for stable expression. Nevertheless, our limited observations using primary human NK cells against 721.221 target cells demonstrated parallels in the kinetics of degranulation and that of target cell killing as observed when using NK cell lines, thus suggesting that primary human NK cells can also kill target cells via minimal degranulation events.

Cytotoxic lymphocytes do represent spectacularly potent immune defenses which are only further emphasized by the degranulation to killing efficiency demonstrated here. Several approaches using NK cells as therapies against established tumors are advancing through clinical and preclinical development (3). A deeper understanding of the degranulation ability of NK cells could help in the refinement of therapy cells, especially in light of this new information that even a single degranulation can be effective in killing. While its was already known that NK degranulation is a highly regulated process (6), the potential reliance of effect upon a single degranulation only emphasizes this further. This efficiency is also in part contributory to the phenomenon of lytic granules convergence towards the MTOC prior to the polarization of the MTOC along with the lytic granules towards the lytic synapse. Our group demonstrated that this convergence process promotes killing of the conjugated target cell while preventing collateral damage to surrounding healthy cells by aggregating the

granules at the target away from potential bystander cells (as would be encountered during immune surveilance) (8). However, in tumor microenvironments, the tumor cells would vastly outnumber an infiltrating NK cell and in this setting the convergence of lytic granules towards a single tumor cell could promote inefficiency in killing the surrounding tumor cells. Thus the strategy of inhibiting convergence of lytic granules and thereby promoting diffuse degranulation has been demonstrated to increase bystander cell killing and has been proposed to increase the efficiency of tumor infiltrating NK cells to cause more widespread local tumor cell killing (8). Our present work suggests were there to be diffuse degranulation in an NK cell within a tumor, even if each surrounding tumor target receives only one or two degranulations, this would be sufficient to cause destruction. While not an intent of this study, the finding further supports the rationale for pursuing undirected degranulation in NK cells and/or in cytotoxic therapy NK cells to improve their intratumoral efficacy. At a minimum we have learned that NK cells are highly potent and efficient in their cytotoxicity and that a single degranulation can mediate target cell destruction.

Supplementary Material

Refer to Web version on PubMed Central for supplementary material.

Acknowledgments

The authors thank Dr. Emily M. Mace and Dr. Alexandre F. Carisey for scientific and technical insight

Funding

This work was supported by NIH (R01AI067946) to Jordan S. Orange and NIH (5T32AI 53831-13/14) to Lavesh A. Gwalani

References

1. Vivier E, Raulet DH, Moretta A, Caligiuri MA, Zitvogel L, Lanier LL, Yokoyama WM, Ugolini S. Innate or Adaptive Immunity? The Example of Natural Killer Cells. Science (80-). 2011; 331:44–49.
2. Lam VC, Lanier LL. NK cells in host responses to viral infections. Curr Opin Immunol. 2017; 44:43–51. [PubMed: 27984782]
3. Guillerey C, Huntington ND, Smyth MJ. Targeting natural killer cells in cancer immunotherapy. Nat Immunol. 2016; 17:1025–1036. [PubMed: 27540992]
4. Krzewski K, Coligan JE. Human NK cell lytic granules and regulation of their exocytosis. Front Immunol. 2012; 3:335. [PubMed: 23162553]
5. Orange JS. Formation and function of the lytic NK-cell immunological synapse. Nat Rev Immunol. 2008; 8:713–725. [PubMed: 19172692]
6. Mace EM, Dongre P, Hsu HT, Sinha P, James AM, Mann SS, Forbes LR, Watkin LB, Orange JS. Cell biological steps and checkpoints in accessing NK cell cytotoxicity. Immunol Cell Biol. 2014; 92:245–255. [PubMed: 24445602]
7. Mentlik AN, Sanborn KB, Holzbaur EL, Orange JS. Rapid lytic granule convergence to the MTOC in natural killer cells is dependent on dynein but not cytolytic commitment. Mol Biol Cell. 2010; 21:2241–56. [PubMed: 20444980]
8. Hsu HT, Mace EM, Carisey AF, Viswanath DI, Christakou AE, Wiklund M, Önfelt B, Orange JS. NK cells converge lytic granules to promote cytotoxicity and prevent bystander killing. J Cell Biol. 2016; 215:875–889. [PubMed: 27903610]

9. Stinchcombe JC, Majorovits E, Bossi G, Fuller S, Griffiths GM. Centrosome polarization delivers secretory granules to the immunological synapse. Nature. 2006; 443:462–465. [PubMed: 17006514]
10. Zhang M, March ME, Lane WS, Long EO. A signaling network stimulated by 2 integrin promotes the polarization of lytic granules in cytotoxic cells. Sci Signal. 2014; 7:ra96–ra96. [PubMed: 25292215]
11. Andzelm MM, Chen X, Krzewski K, Orange JS, Strominger JL. Myosin IIA is required for cytolytic granule exocytosis in human NK cells. J Exp Med. 2007; 204:2285–91. [PubMed: 17875677]
12. Liu D, Xu L, Yang F, Li D, Gong F, Xu T. Rapid biogenesis and sensitization of secretory lysosomes in NK cells mediated by target-cell recognition. Proc Natl Acad Sci U S A. 2005; 102:123–127. [PubMed: 15618404]
13. Liu D, Martina JA, Wu XS, Hammer JA, Long EO. Two modes of lytic granule fusion during degranulation by natural killer cells. Immunol Cell Biol. 2011; 89:728–38. [PubMed: 21483445]
14. Bhat R, Watzl C. Serial Killing of Tumor Cells by Human Natural Killer Cells – Enhancement by Therapeutic Antibodies. PLoS One. 2007; 2:e326. [PubMed: 17389917]
15. Brunner KT, Mauel J, Cerottini JC, Chapuis B. Quantitative assay of the lytic action of immune lymphoid cells on 51-Cr-labelled allogeneic target cells in vitro; inhibition by isoantibody and by drugs. Immunology. 1968; 14:181–96. [PubMed: 4966657]
16. Chattopadhyay PK, Gierahn TM, Roederer M, Love JC. Single-cell technologies for monitoring immune systems. Nat Immunol. 2014; 15:128–135. [PubMed: 24448570]
17. Aktas E, Kucuksezer UC, Bilgic S, Erten G, Deniz G. Relationship between CD107a expression and cytotoxic activity. Cell Immunol. 2009; 254:149–154. [PubMed: 18835598]
18. Alter G, Malenfant JM, Altfeld M. CD107a as a functional marker for the identification of natural killer cell activity. J Immunol Methods. 2004; 294:15–22. [PubMed: 15604012]
19. Betts MR, Brenchley JM, Price DA, De Rosa SC, Douek DC, Roederer M, Koup RA. Sensitive and viable identification of antigen-specific CD8+ T cells by a flow cytometric assay for degranulation. J Immunol Methods. 2003; 281:65–78. [PubMed: 14580882]
20. Rak GD, Mace EM, Banerjee PP, Svitkina T, Orange JS. Natural Killer cell lytic granule secretion occurs through a pervasive actin network at the immune synapse. PLoS Biol. 2011; 9
21. Mace EM, Wu WW, Ho T, Mann SS, Hsu HT, Orange JS. NK Cell Lytic Granules Are Highly Motile at the Immunological Synapse and Require F-Actin for Post-Degranulation Persistence. J Immunol. 2012; 189:4870–4880. [PubMed: 23066148]
22. Sanborn KB, Rak GD, Maru SY, Demers K, Difeo A, Martignetti JA, Betts MR, Favier R, Banerjee PP, Orange JS. Myosin IIA Associates with NK Cell Lytic Granules to Enable Their Interaction with F-Actin and Function at the Immunological Synapse. J Immunol. 2009; 182:6969–6984. [PubMed: 19454694]
23. Bouchier-Hayes L, Muñoz-Pinedo C, Connell S, Green DR. Measuring apoptosis at the single cell level. Methods. 2008; 44:222–228. [PubMed: 18314052]
24. Chung S, Nguyen V, Lin YL, Kamen L, Song A. Thaw-and-use target cells pre-labeled with calcein AM for antibody-dependent cell-mediated cytotoxicity assays. J Immunol Methods. 2016; 447:37–46.
25. Gillissen MA, Yasuda E, de Jong G, Levie SE, Go D, Spits H, van Helden PM, Hazenberg MD. The modified FACS calcein AM retention assay: A high throughput flow cytometer based method to measure cytotoxicity. J Immunol Methods. 2016; 434:16–23. [PubMed: 27084117]
26. Jang YY, Cho D, Kim SK, Shin DJ, Park MH, Lee JJ, Shin MG, Shin JH, Suh SP, Ryang DW. An improved flow cytometry-based natural killer cytotoxicity assay involving calcein AM staining of effector cells. Ann Clin Lab Sci. 2012; 42:42–49. [PubMed: 22371909]
27. Roden MM, Lee KH, Panelli MC, Marincola FM. A novel cytolysis assay using fluorescent labeling and quantitative fluorescent scanning technology. J Immunol Methods. 1999; 226:29–41. [PubMed: 10410969]
28. Yodoi J, Teshigawara K, Nikaido T, Fukui K, Noma T, Honjo T, Takigawa M, Sasaki M, Minato N, Tsudo M. TCGF (IL 2)-receptor inducing factor(s). I. Regulation of IL 2 receptor on a natural killer-like cell line (YT cells). J Immunol. 1985; 134:1623–1630. [PubMed: 2578514]

29. Somanchi SS, McCulley KJ, Somanchi A, Chan LL, Lee DA. A novel method for assessment of natural killer cell cytotoxicity using image cytometry. PLoS One. 2015; 10
30. Gong JH, Maki G, Klingemann HG. Characterization of a human cell line (NK-92) with phenotypical and functional characteristics of activated natural killer cells. Leukemia. 1994; 8:652–8. [PubMed: 8152260]
31. Guldevall K, Vanherberghen B, Frisk T, Hurtig J, Christakou AE, Manneberg O, Lindström S, Andersson-Svahn H, Wiklund M, Önfelt B. Imaging immune surveillance of individual natural killer cells confined in microwell arrays. PLoS One. 2010; 5:e15453. [PubMed: 21103395]
32. McCann FE, Vanherberghen B, Eleme K, Carlin LM, Newsam RJ, Goulding D, Davis DM. The size of the synaptic cleft and distinct distributions of filamentous actin, ezrin, CD43, and CD45 at activating and inhibitory human NK cell immune synapses. J Immunol. 2003; 170:2862–2870. [PubMed: 12626536]
33. Vanherberghen B, Olofsson PE, Forslund E, Sternberg-Simon M, Khorshidi MA, Pacouret S, Guldevall K, Enqvist M, Malmberg KJ, Mehr R, Önfelt B. Classification of human natural killer cells based on migration behavior and cytotoxic response. Blood. 2013; 121
34. Choi PJ, Mitchison TJ. Imaging burst kinetics and spatial coordination during serial killing by single natural killer cells. Proc Natl Acad Sci U S A. 2013; 110:6488–93. [PubMed: 23576740]
35. Netter P, Anft M, Watzl C. Termination of the Activating NK Cell Immunological Synapse Is an Active and Regulated Process. J Immunol. 2017; 199:ji1700394.
36. Chang HF, Bzeih H, Schirra C, Chitirala P, Halimani M, Cordat E, Krause E, Rettig J, Pattu V. Endocytosis of Cytotoxic Granules Is Essential for Multiple Killing of Target Cells by T Lymphocytes. J Immunol. 2016; 197:2473–84. [PubMed: 27527597]
37. Liu D, Bryceson YT, Meckel T, Vasiliver-Shamis G, Dustin ML, Long EO. Integrin-Dependent Organization and Bidirectional Vesicular Traffic at Cytotoxic Immune Synapses. Immunity. 2009; 31:99–109. [PubMed: 19592272]
38. Ming M, Schirra C, Becherer U, Stevens DR, Rettig J. Behavior and Properties of Mature Lytic Granules at the Immunological Synapse of Human Cytotoxic T Lymphocytes. PLoS One. 2015; 10:e0135994. [PubMed: 26296096]
39. Lyubchenko TA, Wurth GA, Zweifach A. Role of calcium influx in cytotoxic T lymphocyte lytic granule exocytosis during target cell killing. Immunity. 2001; 15:847–859. [PubMed: 11728345]
40. Stinchcombe JC, Bossi G, Booth S, Griffiths GM. The immunological synapse of CTL contains a secretory domain and membrane bridges. Immunity. 2001; 15:751–761. [PubMed: 11728337]
41. Umemoto M, Azuma E, Hirayama M, Nagai M, Hiratake S, Qi J, Kumamoto T, Komada Y, Sakurai M. Two cytotoxic pathways of natural killer cells in human cord blood: implications in cord blood transplantation. Br J Haematol. 1997; 98:1037–40. [PubMed: 9326208]
42. Zychlinsky A, Zheng LM, Liu CC, Young JD. Cytolytic lymphocytes induce both apoptosis and necrosis in target cells. J Immunol. 1991; 146:393–400. [PubMed: 1984450]
43. Brown ACN, Oddos S, Dobbie IM, Alakoskela JM, Parton RM, Eissmann P, Neil MAA, Dunsby C, French PMW, Davis I, Davis DM. Remodelling of cortical actin where lytic granules dock at Natural Killer cell immune synapses revealed by super-resolution microscopy. PLoS Biol. 2011; 9:e1001152. [PubMed: 21931537]
44. Beal AM, Anikeeva N, Varma R, Cameron TO, Vasiliver-Shamis G, Norris PJ, Dustin ML, Sykulev Y. Kinetics of Early T Cell Receptor Signaling Regulate the Pathway of Lytic Granule Delivery to the Secretory Domain. Immunity. 2009; 31:632–642. [PubMed: 19833088]
45. Carisey AF, Mace EM, Saeed MB, Davis DM, Orange JS. Nanoscale Dynamism of Actin Enables Secretory Function in Cytolytic Cells. Curr Biol. 2018; 28:489–502.e9. [PubMed: 29398219]
46. Ritter AT, Kapnick SM, Murugesan S, Schwartzberg PL, Griffiths GM, Lippincott-Schwartz J. Cortical actin recovery at the immunological synapse leads to termination of lytic granule secretion in cytotoxic T lymphocytes. Proc Natl Acad Sci. 2017; 114:E6585–E6594. [PubMed: 28716933]
47. Drexler HG, Matsuo Y. Malignant hematopoietic cell lines: in vitro models for the study of natural killer cell leukemia-lymphoma. Leukemia. 2000; 14:777–82. [PubMed: 10803505]

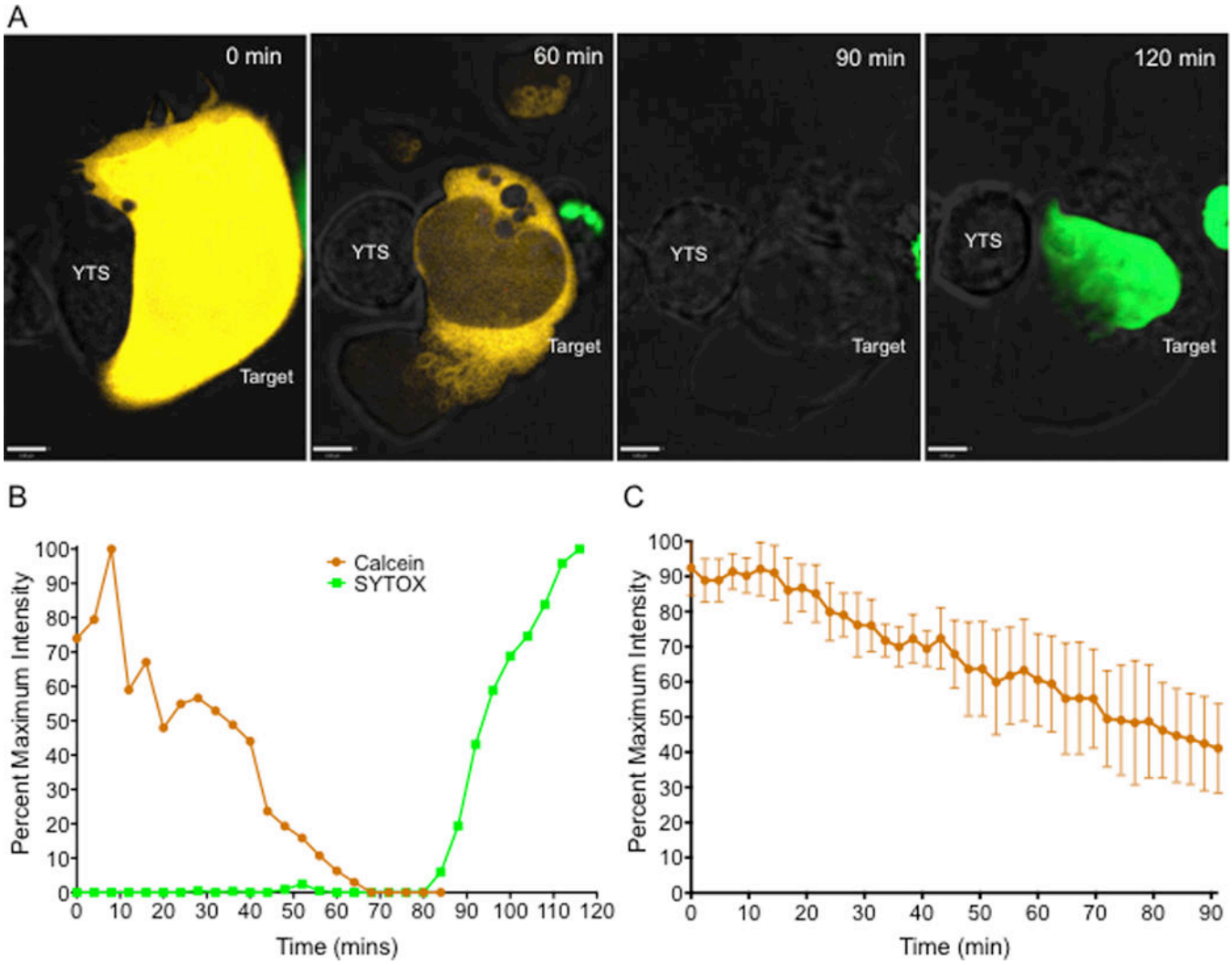

Figure 1. Loss of calcein fluorescence is an early indicator of target cell death

(A and B) YTS effector cells were incubated with calcein, orange-red labeled 721.221 target cells (yellow) in the presence of SYTOX Green nucleic acid stain (green). Z stack images of single cell YTS-721.221 conjugates were acquired by confocal microscopy. Imaging was performed at a frame rate of one image every 4 minutes for 120 minutes to 180 minutes until target cell death was observed. (A) Representative maximum projection time-lapse images of the YTS-721.221 conjugate. Scale bar 5μm. Target cell death was detected either through loss of calcein from the target cell or through entry of SYTOX Green in to the target cell. (B) Quantitative analysis of calcein and SYTOX Green fluorescence in the 721.221 target cell from the representative live cell cytotoxicity assay shown in (A). Values are percentage of maximum fluorescence intensity of the dyes in the target cell during the imaging time frame. Results are representative of at least 5 independent experiments. (C) Quantitative analysis of loss of calcein fluorescence in 721.221 target cells incubated without NK cells. Analyses shown are from 6 independent experiments (n=9). Data are represented as mean +/− standard deviation (SD).

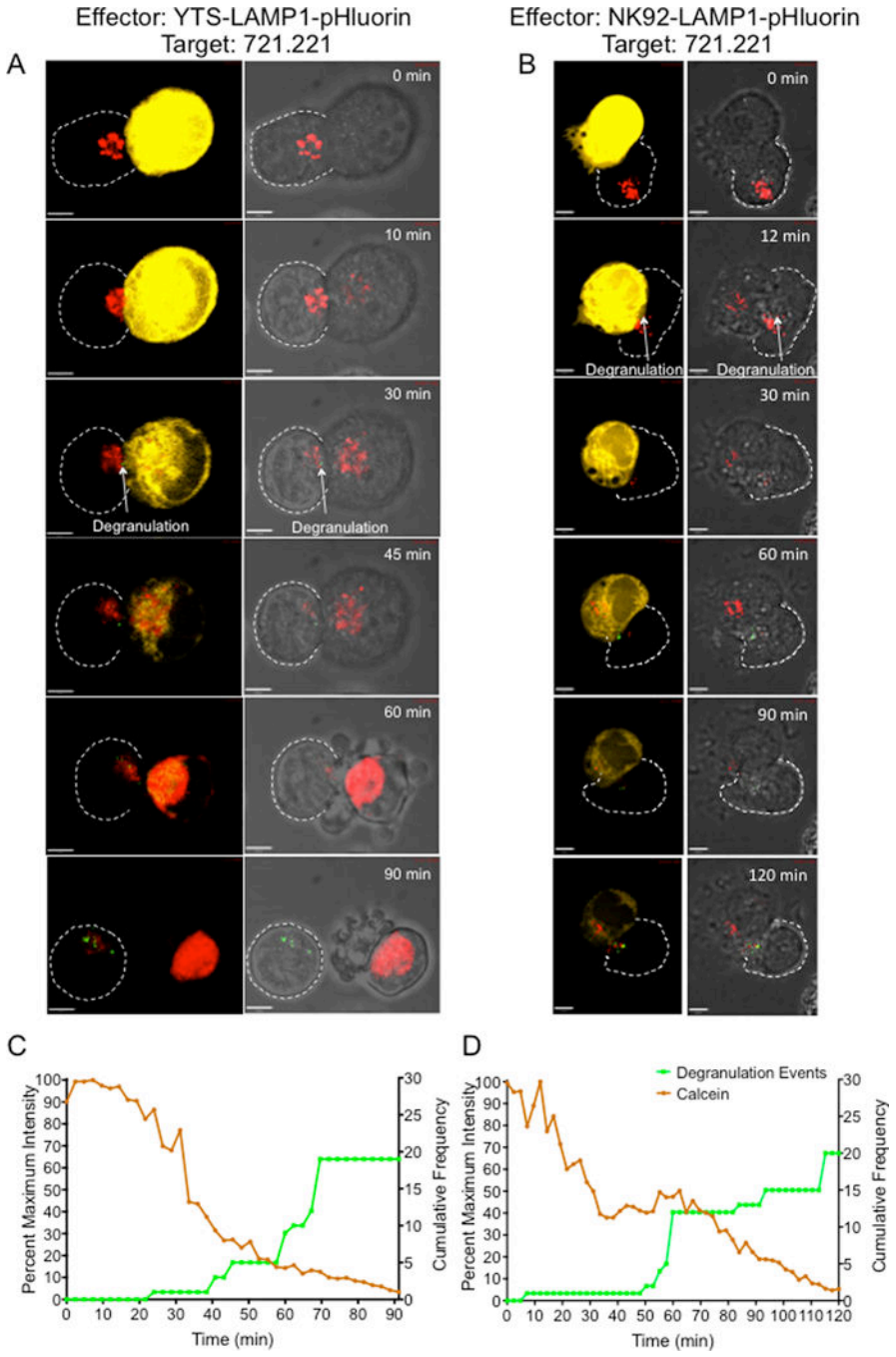

Figure 2. Live single-cell cytotoxicity for visualization and measurement of target cell killing by NK cells

LAMP1-pHluorin transduced YTS and NK92 (effector) cells were loaded with LysoTracker Deep Red (red) and incubated with calcein, AM orange-red labeled 721.221 target cells (yellow). Z-stack images of single cell conjugates were acquired by confocal microscopy. Even though the 721.221 target cells were not stained with LysoTracker™ Deep Red, the excess dye from effector cells that leaked in to the medium was taken up by the target cell and the accumulation in the target cell increased once the membrane integrity was lost. Imaging was performed at a frame rate of 1 image every 2.4 minutes for 90 to 120 minutes

until target cell death was observed. Representative maximum projection time-lapse image sequences of a single YTS cell (A) and a NK92 cell (B) conjugated to a single 721.221 target cell. Left panel shows calcein fluorescence (yellow) and degranulation events (green) at the NK-target cell synapse. Right panels show bright field images of the conjugates showing degranulation events (green) and characteristic apoptotic membrane blebbing in the target cell. The synaptic region of interest were selected as the overlapping region between the NK and the target cell identified in bright field images. Scale bar 5μm. (C and D) Quantitative analysis of degranulation and calcein fluorescence in the representative YTS-721.221 conjugate (C) and NK92-721.221 conjugate (D). Cumulative frequency of degranulation events in the effector cells and the fluorescence intensity of calcein in the target cell (calculated as a percent of maximum fluorescence intensity) were plotted against imaging time. Images and analyses are representative of 10-15 independent experiments.

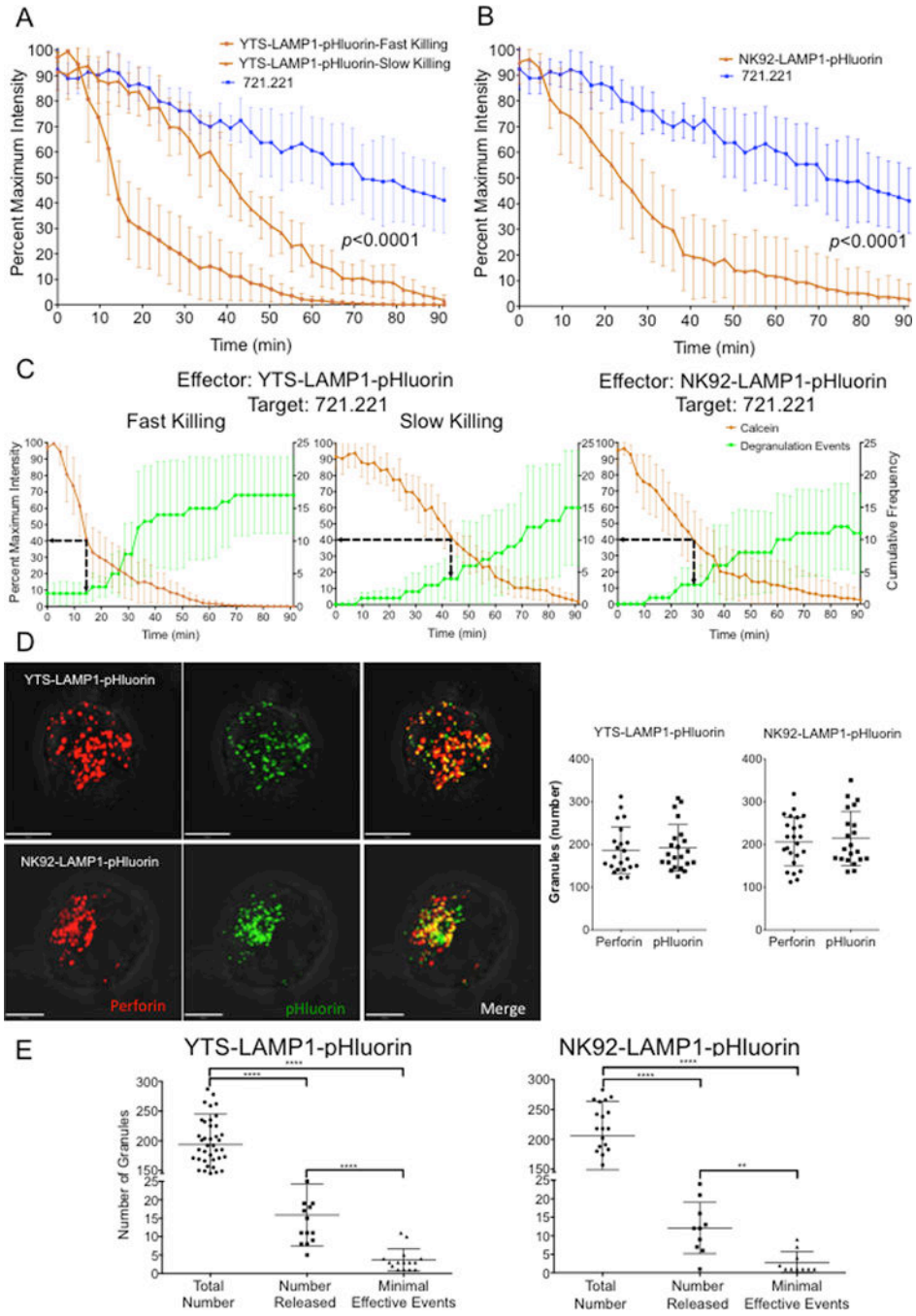

Figure 3. Quantitative analysis of degranulation during NK cell mediated killing of target cells in live single cell cytotoxicity assays

(A) Analysis of calcein fluorescence in 721.221 target cells conjugated to YTS cells showed either a slow release or a fast release pattern. Both curves were significantly different from each other. (B) Analysis of calcein fluorescence in 721.221 target cells conjugated to NK92 cells showed a single pattern of calcein release. In both (A) and (B) loss of calcein fluorescence from 721.221 cells conjugated to NK effector cells were significantly different from loss of calcein fluorescence seen in 721.221 cells incubated without effector cells (data from Figure 1C). Statistical analysis was done by log transformation of the mean

fluorescence data, linear regression analysis of the transformed data and comparison of slopes; $p<0.0001$ for all comparisons. (C) Average minimal effective degranulation events for cytotoxicity were determined for the different patterns of killing observed. Minimal effective degranulation was defined as the number of degranulation events in the effector cells corresponding to 60% loss of calcein fluorescence in target cells (dashed arrow). Data from A, B and C are represented as mean values +/− SD. Data are from 5 to 15 independent experiments in each group. (D) Representative extended focus confocal images and quantitative analysis of the total number of granules in LAMP1-pHluorin transduced YTS and NK92 NK cell lines. Lytic granules were counted either using the perforin signal or the LAMP-1-pHluorin signal. (E) Total number of lytic granules (determined using perforin staining), the number of lytic granules released in the synaptic region during live cell imaging and the minimal effective degranulation events needed for cytotoxicity against 721.221 target cells. Data are represented as mean values ± SD. Data are from 25 single cells to determine total number of granules and from 10 to 15 independent experiments to determine the number lytic granules released and minimal effective degranulation events. Statistical analysis were done using unpaired Student's t test to compare total number to number released and minimal effective events and paired Student's *t* test to compare number released and minimal effective events. $^{**}p<0.01$; $^{****}p<0.0001$.

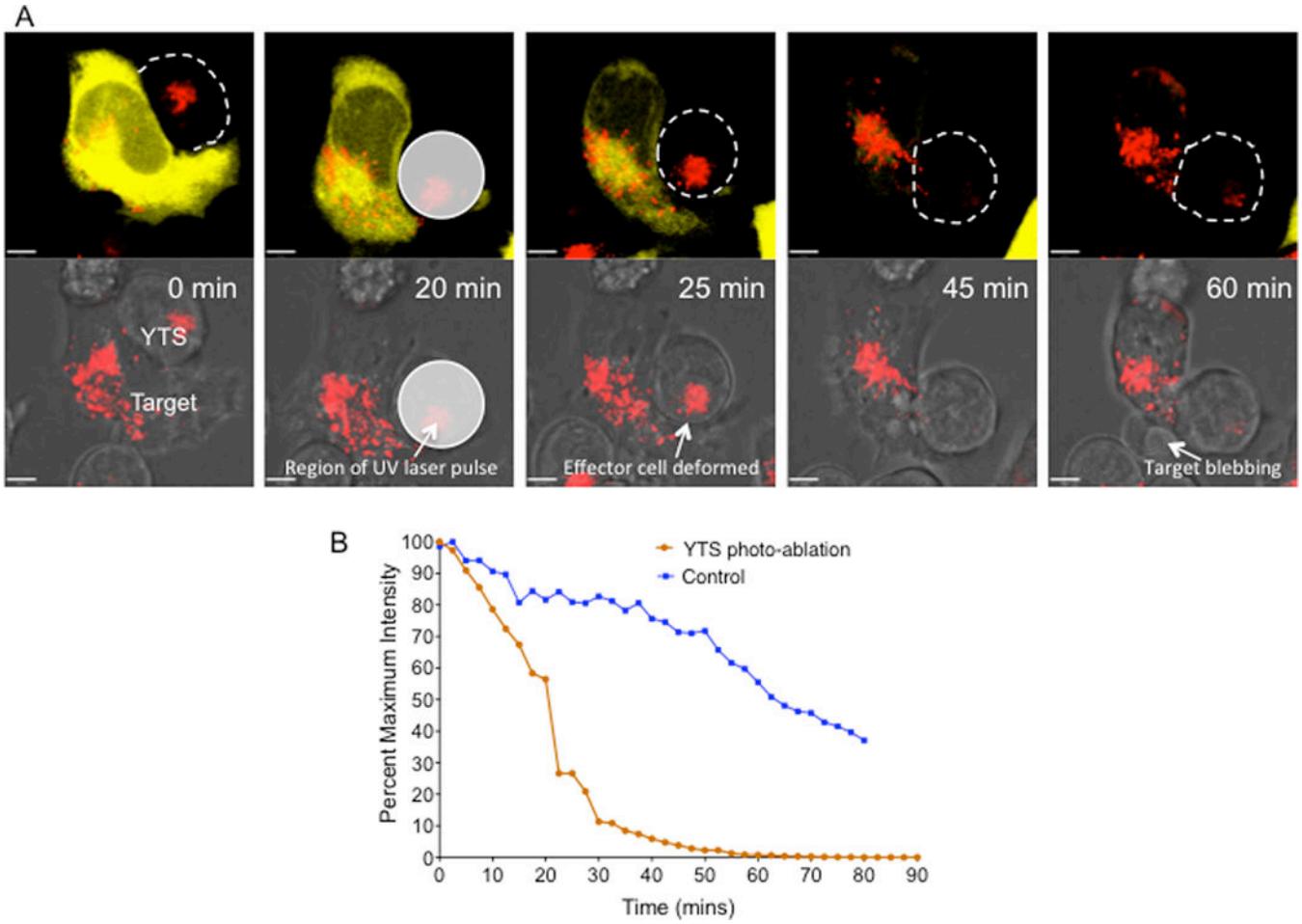

Figure 4. Initial degranulations in a NK cell are sufficient to kill the target cell

YTS effector cells stained with LysoTracker™ Deep Red (red) were incubated with calcein, orange-red labeled 721.221 target cells (yellow). Z-stack images of single YTS-721.221 cell conjugates were acquired at a frame rate of one image every 2.5 minutes. UV laser pulses were applied in the region of the YTS cell for photo-ablation of the effector NK cell once the lytic granules were polarized towards the target cell and the target cell had begun to lose its calcein fluorescence. In control experiments the YTS cell was photo-ablated at an earlier time point before polarization of the lytic granules towards the IS. (A) Representative maximum projection time-lapse images of the YTS-721.221 conjugate. Top panel shows calcein fluorescence (yellow); Bottom panel shows bright field images of the conjugate with deformation of the YTS NK cell after photo-ablation and characteristic apoptotic membrane blebbing in the target cell. The translucent white circle show the boundries of the region in which the UV pulses were applied to photo-ablate the YTS cell. Scale bar 5μm. (B) Quantitative analysis of calcein fluorescence in the 721.221 target cell from the representative live cell cytotoxicity assay shown in (A) and from a control experiment in which UV laser pulses were applied to YTS cell before the lytic granules had polarized. Images and analysis is representative of at least 5 independent experiments.

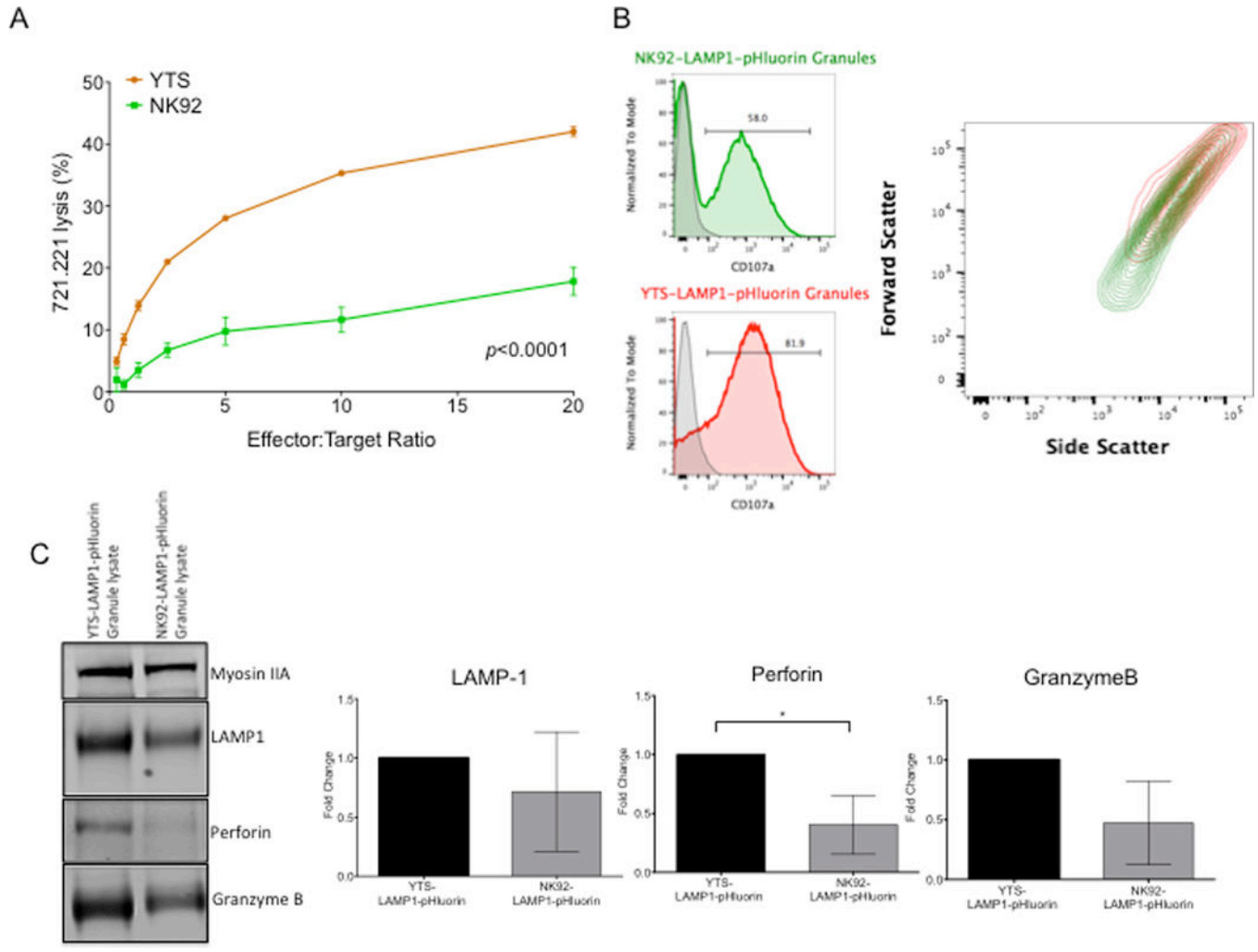

Figure 5. Cytotoxic efficiency and lytic granule characteristics of LAMP-1-pHluorin transduced NK cell lines YTS and NK92

(A) Cytotoxic activity of YTS-LAMP-1-pHluorin and NK92-LAMP-1-pHluorin cells against their target cell line 721.221 in a 4-hour ^{51}Cr release cytotoxicity assay. Experiments were performed in triplicates. Data represents mean +/− SEM from 3 independent experiments. (B) Lytic granules were isolated from the NK cell lines by density gradient ultracentrifugation. Isolated lytic granules were permeabilized, fixed and stained with anti-LAMP1 antibody for flow cytometry analysis. LAMP-1 positive events were gated for comparison of their relative sizes by their ability to scatter light. Overlay of forward and side scatter plots of the granules from the two cell lines showed that YTS granules (red) were relatively larger than the NK92 granules (green). (C) Western blots and densitometry analysis of lytic granule lysates from the LAMP-1-pHluorin transduced NK cell lines YTS and NK92. Densitometry values of the LAMP1, Perforin and GranzymeB bands were normalized to Myosin IIA and plotted as a proportion of effector molecule content in YTS lytic granules. Data in (B) is representative of 3 independent experiments. Data in (C) is average of 3 independent experiments, normalized to Myosin IIA, and plotted as fold change

relative to YTS lytic granules Error bars represent ±SD. Statistical analysis were performed using unpaired Student's *t* test of log transformed densitometry data. *$p<0.05$

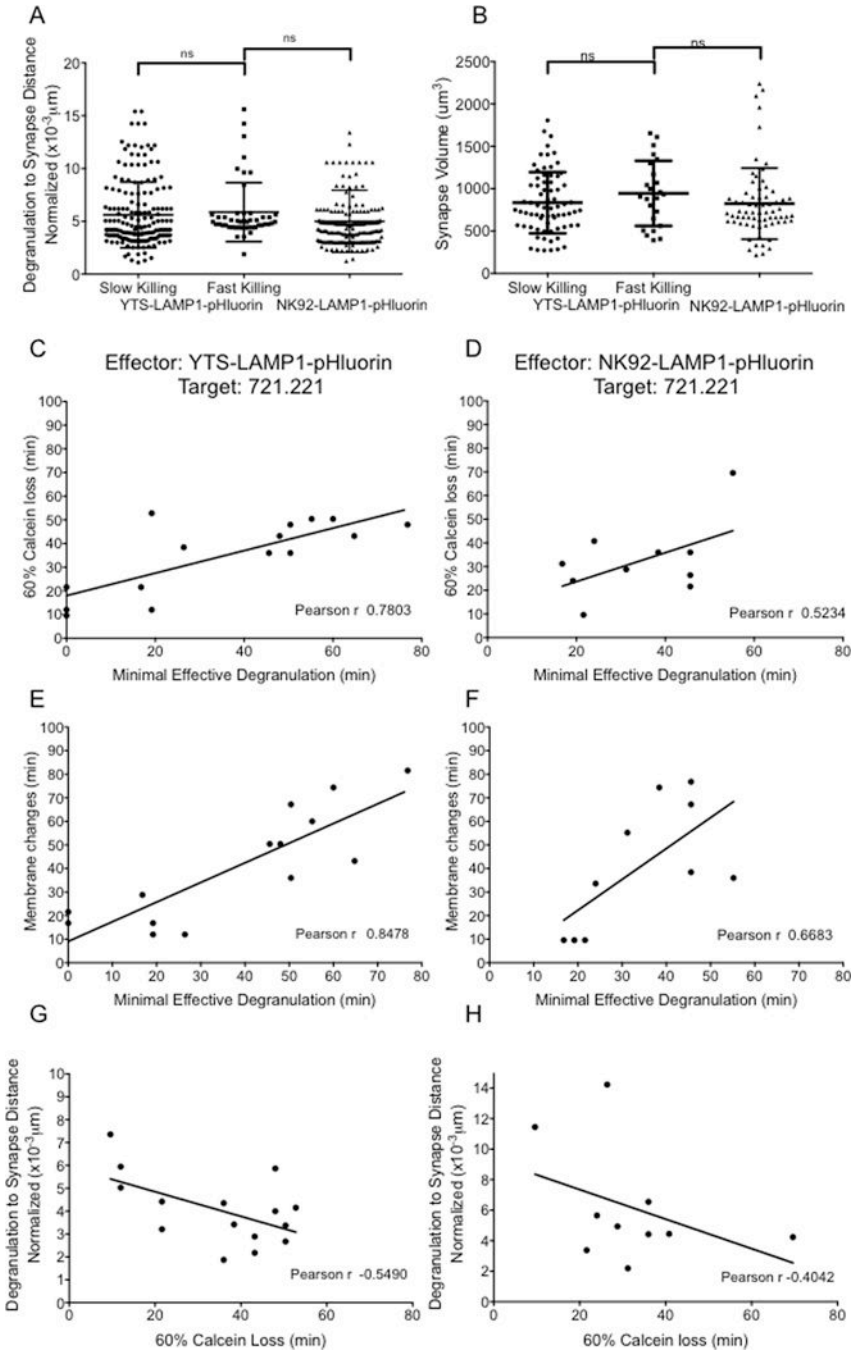

Figure 6. Spatiotemporal association between degranulation and NK cell cytotoxicity

(A) Synapse to degranulation distances and synapse sizes were measured from time-lapse imaging data of YTS-721.221 and NK92-721.221 conjugates illustrated in Figure 3. Mean distances between degranulation events and the centroid of the synapse were measured at each time point of the time-lapse images until target cell death was observed. Normalization of the data was performed by dividing absolute granule to synapse distances by the size of the synapse at the respective time point. (B) Synapse sizes were measured by drawing a ROI in the region of overlap between the NK and target cells at each time point of the time-lapse

images until target cell death was observed. Dots in (A) and (B) represent data from each time point of live cell imaging from 5 to 10 independent experiments in each group. Lines indicate mean values +/− SD. (C and D) Correlation between time to commitment to target cell death (defined as time point after which loss of calcein fluorescence in the target cell exceeded 60%) and time to reach minimal effective degranulation (defined as time point at which the cumulative frequency of degranulation events reached the average minimal effective level). (E and F) Correlation between membrane changes in the target cell (marked by formation of blebs observed in the bright field channel) and time to reach minimal effective degranulation events. (G and H) Correlation between average degranulation to synapse distance for each conjugate (normalized as above) and time to commitment to target cell death. Dots in (C, D, E, F, G and H) represent data from time-lapse imaging experiments illustrated in Figure 3. Pearson's correlation coefficient was determined for the fitted line in each plot. A single data point in (E) and (G) was determined to be an outlier (value exceeded 1.5xInterquartile Range) and was removed from correlation analysis.